Diamond & Related Materials 102 (2020) 107687

Contents lists available at ScienceDirect

Diamond & Related Materials

journal homepage: www.elsevier.com/locate/diamond

N, S codoped activated mesoporous carbon derived from the Datura metel seed pod as active electrodes for supercapacitors

F. Regan Maria Sundar Raj[a,c,*], G. Boopathi[b], N. Victor Jaya[a], D. Kalpana[d], A. Pandurangan[b]

[a] High Pressure and Nanoscience Laboratory, Department of Physics, Anna University, Chennai 600 025, Tamil Nadu, India
[b] Department of Chemistry, Anna University, Chennai 600 025, India
[c] Jeppiaar Engineering College, Department of Physics, Chennai 600 119, India
[d] Central Electrochemical Research Institute, Madras Unit, CSIR Madras Complex, Taramani, Chennai 600 113, India

ARTICLE INFO

Keywords:
Datura metel seed pod
KOH
Thiourea
Mesoporous
Carbon matrix

ABSTRACT

A successful transformation of Datura metel seed pod into activated carbon (AC) codoped with nitrogen (N) and sulfur (S) contents have opened up a new route in this process which turned the material to be source material for supercapacitor application. The appropriate proportion of KOH with raw material and the activation condition were the key factors in this conversion process. The conversion of Datura metel seed pod into AC has opened the possibility of the material for supercapacitor application. HRSEM/EDX with elemental mapping and XPS analysis evidenced the morphologies and codoped surface functionalities. XRD, Raman spectra and N_2 adsorption/desorption isotherm analysis were studied. The activation temperature 600 °C for 1 h with 30 wt% of KOH resulting the surface area of the derived AC (DM 3) is found to be 795.4857 m^2/g. The codoped surface functionalities have led to a significant specific capacitance of 340 F/g at a current density of 1 A/g. The novel material exhibits excellent cycling stability with 95.24% capacitance retention at 1 A/g for 3000 cycles proved to be an excellent electrode material for energy storage especially for supercapacitor application.

1. Introduction

Immoderate consumption of fossil fuels attains faster than huge energy challenges and the level of rise in climate-warming, carbon dioxide (CO_2) in the atmosphere is a near-record. The amount of these issues and practical concerns of modern life in our planet prompted an increasing in the number of researchers, countries and companies are embracing the global production of renewable energy coming from solar radiation, wind energy, recent forms of waste-to-biomass translation assembly leading to biofuel energy and other sources of alternative energies [1–5]. For adapting global technologies, we require reliable electric energy-storage systems. The electric energy-storage devices store energy electrochemically in supercapacitors (ultracapacitors) and traditional lithium-ion batteries [6–10]. Though batteries are enriched for higher energy density, but their power density factors low down with deprived cycle life makes hamper for high power demanding applications such as hybrid electrical vehicles, cranes, drivetrains, other transport system and in opening urgent situation doors systems [11–14]. By disparity, supercapacitor can store better amount of energy than the conventional capacitors and a better choice to provide energy far quicker than batteries [15]. Hence, supercapacitor lucratively meets the demands for portable electronics in electric vehicles bridges an ideal energy-storage device. The mechanism of charge-storage in supercapacitors, can be explained by the following possibilities [6,16,17] EDLC (electric double layer capacitance) storage system relies on the non-Faradaic reaction at electrode/electrolyte interface in which a variety of bioderived activated carbon (AC) materials are used as electrode materials and pseudocapacitance system relies on the reversible Faradaic redox reactions at electroactive surfaces in which certain metal oxides or conducting polymer based are used as electrode materials [18,19]. However, the demands and cost of the device are vital for large-scale industries choice. On account of these commercial available supercapacitors relies on AC for their low cost and high surface area [20–24] as electrode materials. To enhance the challenges mentioned above, researchers explored activated carbon materials from various biomasses have especially used for electrode materials [25–28]. Among them, a derived AC is utilized as electrode material for supercapacitor due to its low cost, high conductivity, surface area, availability and possessing better properties [29–31].

Nowadays, more and more researchers are focused on utilization of biomass materials as they are abundant, clean and renewable. Hence, biomass-derived porous carbon materials can be used as an inexpensive

* Corresponding author at: High Pressure and Nanoscience Laboratory, Department of Physics, Anna University, Chennai 600 025, Tamil Nadu, India.
E-mail address: regan.physics@gmail.com (F.R.M.S. Raj).

https://doi.org/10.1016/j.diamond.2019.107687
Received 9 September 2019; Received in revised form 6 December 2019; Accepted 26 December 2019
Available online 28 December 2019
0925-9635/ © 2019 Elsevier B.V. All rights reserved.

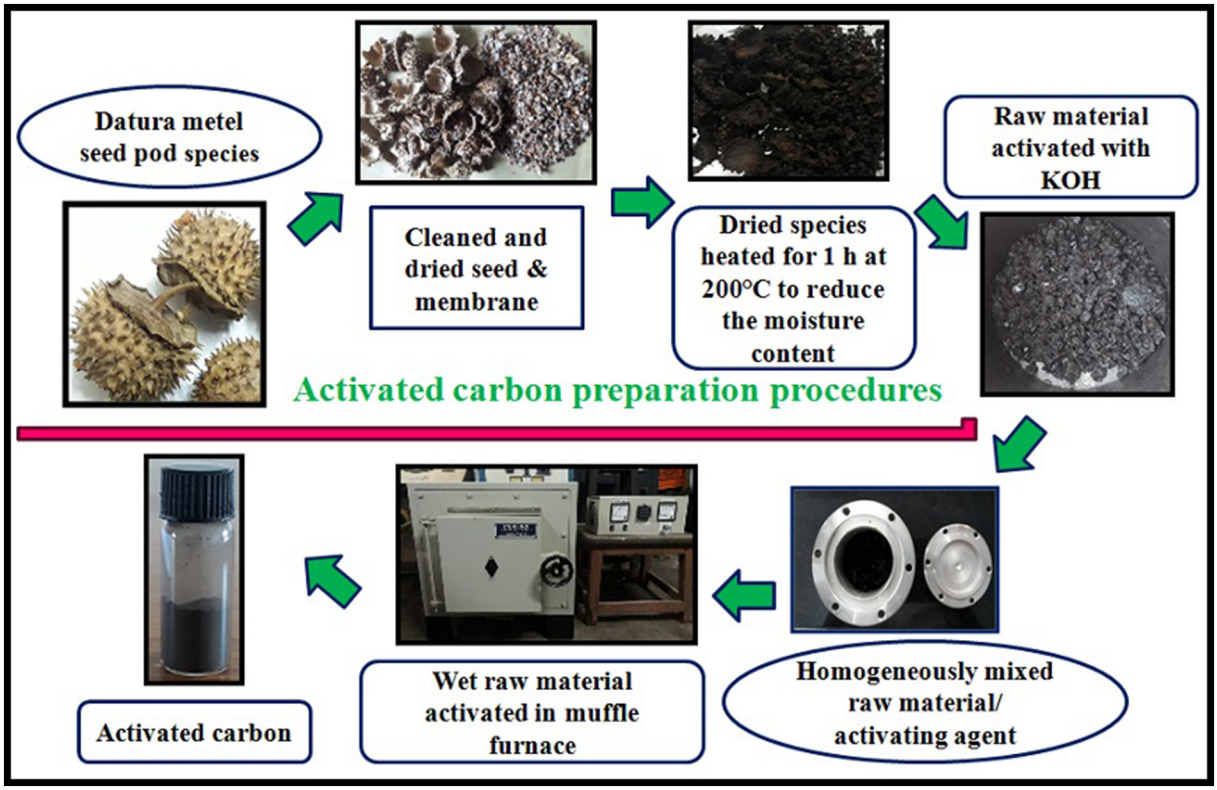

Fig. 1. Schematic illustration of the step procedures for preparing a highly porous carbon with Datura metel seed pod as starting materials.

source of carbon for the production of high added-value products [32–35]. More important, its high electrical conductivity influences the electrochemical performances. The carbon-based electrode materials of double-layer capacitors accelerate the energy-storage of supercapacitors, features the capacitance property relationship reported in the literature. The activation process of the electrode material include activation temperature, chemical activating agents, ratio of activating agent and holding time are important for high yield material and well-developed pores [36–45]. The electrode material with modulated surface areas and pore-size must be greater than electrolyte ion to have significant increase in capacitance, as the distributions of pores distinguished as micropores, mesopores and macropores in the size range from < 2, 2–50 and > 50 nm to smooth the progress of access and adsorption of the ions on the surface of electrode materials to store charges, enhancing the electrode material gapping between batteries and conventional capacitors providing high power supercapacitor [46,47].

Besides the pore-size distribution of electrode materials, the surface functionalities also play important roles in the chemical storage systems, by embellishment with various kinds of functionalities foremost to the reactions between the functionalities and protons in the electrolyte, enhances the surface-active sites promote energy-storage applications [48]. The S and N codoped AC is favored in fine-tuning the electronic structure of the carbonaceous material leading to change in electron density of states, increasing electrode-electrolyte interaction, conductivity shows an excellent specific capacitance [49]. The O functionalities also have important effects in enhancing the material surface wettability by increasing the hydrophilic polar sites. Other surface functionalities such as boron (B), fluorine (F) and phosphorus (P) doped into the carbon matrix enable additional surface pseudocapacitance in carbon materials [50]. The current collector used in electrochemical study offers the enhanced contact impedance between the active film and the current collector, especially for activated carbon-based material the carbon-felt is used as current collector in aqueous electrolytes providing higher ionic conductivity, flexibility and does not corrode, led to improve electrochemical stability at wide potentials [51].

Datura is an herbaceous perennial or annual shrubby plant, which is grown in tropical region. The species are also known by other common names such as Devil's snare etc. The plant consists of stem, broad leaf, flower and seed [52]. Herein, we employ our attention on the viability of using an abundant Datura metel seed pod as carbon precursor in a simplistic technique for the large-scale yield of AC. The pioneering work of employing Datura metel seed pod in synthesizing the N, S co-doped AC for supercapacitor application is established. To the pre-eminent of our information, no studies are reported on Datura metel seed pod based porous carbon for supercapacitors application.

2. Experimental

2.1. Sample preparation

The Datura metel seed pod is used as the raw material for the sample preparation. The DM materials were synthesized as follows: The seed pod was washed thrice using deionized water to remove dust and other particles. The cleaned pieces were dried in an oven at 100 °C to removal of water bodies present in the raw material. Further, the temperature is raised to 200 °C and maintained in the same condition for 1 h to reduce the moisture content present in the raw material. The carbonized sample was then ground in to small particles using mortar pestle. The charcoal was activated by mixing the above prepared raw material and agitated with potassium hydroxide (KOH) of 30 wt% aqueous solution. The impregnation ratio kept as 2:1 (KOH: carbon), respectively. 1 M of thiourea added for N and S source in the AC. The mixture was mixed homogeneously at ambient condition with occasional stirring for 24 h. Finally, the mixture was filled into a stainless steel autoclave for obtaining porous carbon. The autoclave sealed with the prepared mixture and kept in a muffle furnace at three different activation temperatures such as 400, 500 and 600 °C at a heating rate of 5 °C/min under vacuum conditions for 1 h to study the activation

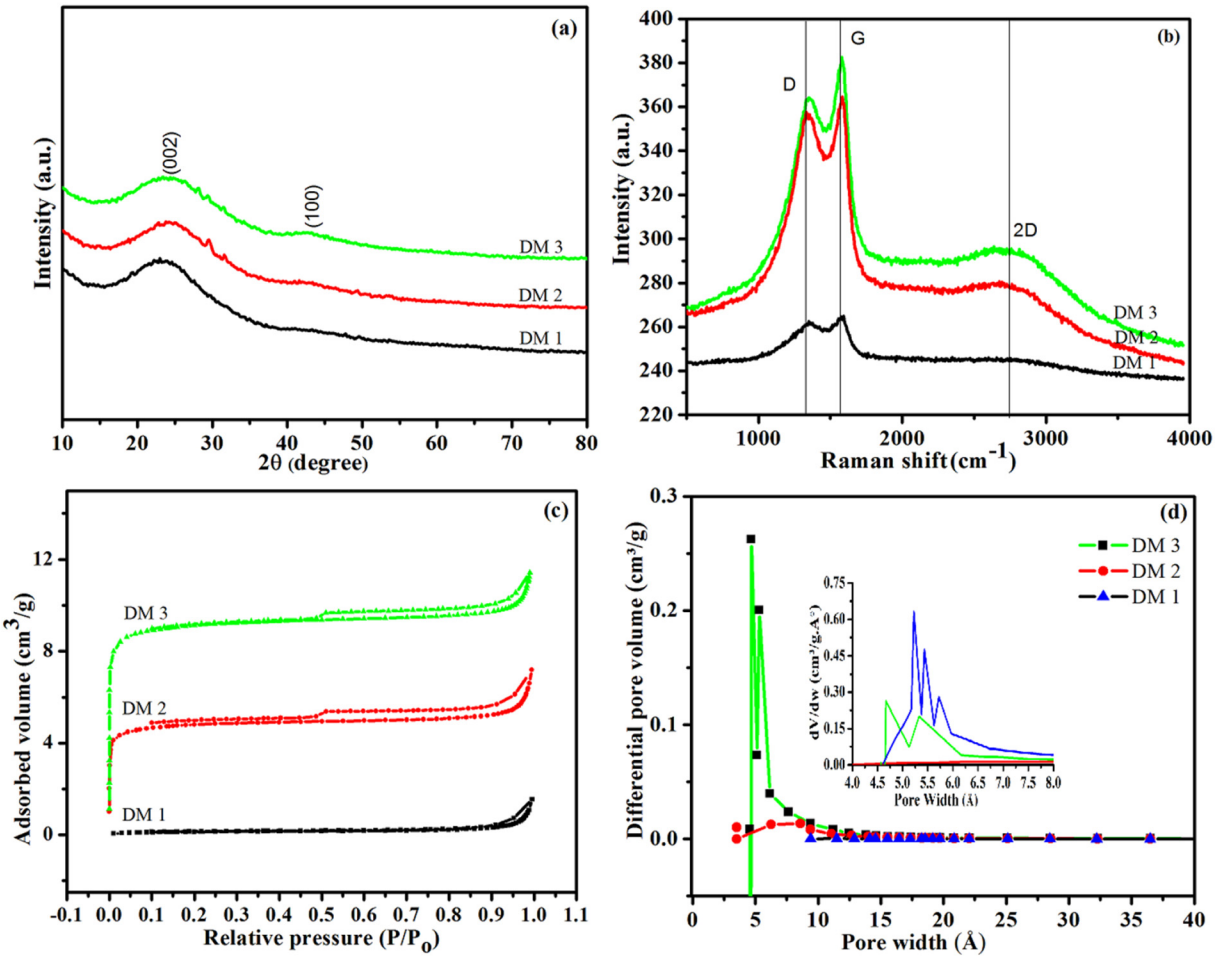

Fig. 2. (a) XRD pattern, (b) Raman spectra, (c) N_2 adsorption − desorption isotherm and (d) pore-size distributions of the AC.

process in AC. Then, the resultant mixture was repeatedly washed with deionized water to eradicate residuals and maintain a neutral pH. The resulting sample was dried in the hot air oven at 60 °C throughout night. The DM series samples synthesized at different activation temperatures enriched with nitrogen and sulfur carbon sources are referred as DM 1, DM 2 and DM 3, respectively. A schematic representation of a highly porous AC with Datura metel seed pod as illustrated in Fig. 1.

2.2. Characterization methods

X-ray diffraction (XRD) measurements were carried out using Bruker AXS D8 attached to an advanced diffractometer (Rigaku) with a CuKα radiation fitted with Lynx Eye detector. The samples were scanned in the range between 10° and 80° with a scan rate of 0.02°/min. Raman spectra were obtained on a (CRM) confocal Raman microscope with an excitation laser beam wavelength of 532 nm (Nd-YAG). N_2 adsorption/desorption isotherms analyzed using ASAP 2020 analyzer at −196.15 °C. The surface area was calculated from the adsorption desorption isotherms using Brunauer-Emmett-Teller (BET) method. The surface morphologies were determined by using high-resolution scanning electron microscope (HRSEM) FEI Quanta FEG 200. The functionalities were investigated through EDX (Energy dispersive X-ray spectrum) fitted with elemental mapping tool. The surface functionalities of the samples were analyzed with X-ray photoelectron spectrometer (CAE: pass energy 120.0 eV of analyzer mode). HRTEM analysis made with JEOL 3010 instrument. The EIS analysis was carried out using BioLogic scientific instruments were conducted in the frequency range of 10 KHz to 1 mHz at an open-circuit potential with an a.c. amplitude of 10 mV.

2.3. Working electrode preparation and electrochemical measurements

All the electrochemical measurements were evaluated in electrochemical workstation using PGSTAT302F (Autolab). The fabrication of working electrodes for the supercapacitors were formulated as follows: Firstly, taking accurately weighed amounts of the active material (80 wt %), conducting black material (10 wt%), and binder polyvinylidene difluoride (PVDf) (10 wt%). Secondly, the weighed electrode material taken in the ratio of 8:1:1 added with few drops of *N, N*-dimethylformamide to form a homogeneous slurry, all the preparation were carried out for about 1 h. Thirdly, the homogeneous slurry was coated on the carbon-felt in the geometric area, 1 × 1 cm^2 by Doctor's blade method. Finally, the slurry coated on the carbon-felt was dried at 80 °C for 12 h in an oven. Electrochemical test were carried out in a three-electrode system in 1 mol/L H_2SO_4 aqueous solution. The carbon-felt coated with codoped activated carbon served as a working electrode material for electrochemical characterization. Ag/AgCl as reference and Pt wire as counter electrode, respectively. The electrochemical properties are evaluated for all DM samples were determined by cyclic voltammetry (CV), galvanostatic charge/discharge (GCD) and electrochemical impedances spectroscopy (EIS). The CV tests of the codoped activated carbon electrodes were carried at various scan rates in the potential window between 0.0 and 1.0 V (vs. Ag/AgCl). GCD curves of the codoped activated carbon electrodes were measured in a potential of 0.0 to 1.0 V, respectively, at different current densities. The specific capacitance of a single electrode was determined using Eq. (1):

$$C = \frac{I \times \Delta t}{m \times \Delta V} \quad (1)$$

where C is the gravimetric capacitance (F/g), I is the discharge current (A), Δt is the discharge time (s), m is the mass of the active material (g) and ΔV is the array of charge-discharge voltage (V).

3. Results and discussion

The X-ray diffraction pattern of the codoped DM samples obtained at 400, 500 and 600 °C are shown in Fig. 2(a). All the samples exhibit a broad diffraction peak around 2θ of 24° represents the (002) reflection plane of graphitic carbon planes of graphitic frameworks [53], attributed to turbostratic stacking [54]. The increases in temperature reflects in increases in peak intensity at (002) plane, especially DM 3 with increase in graphitic stacking order [55]. In addition, a small spike noticed at a broad diffraction peak around 2θ of 28° indicates a graphitic order [56]. Another peak centered at 44° assigned to the (100) diffraction plane is relatively low in intensity. The intensity of (100) plane increases, resulting in formation of superior degree of graphitic structure at superior activation temperature. These obtained nano-graphitic structures will significantly get better with electrical conductivity [57–61].

Raman spectroscopy is an influential assesses to detect the structure and quality information on the degree of graphitized carbon materials. As shown in Fig. 2(b) which shows three absorbance region: The region observed at 1350 cm^{-1} is mainly attributed to the D band arises from disordering degree in the structure (C—C). The region centered nearly at 1578 cm^{-1} is due to the G-band originates from the vibrations of sp^2-hybridized carbon. The peak obtained at 2732 cm^{-1} is a characteristic region of 2D-band [62–64]. The intensity ratio of G to D bands is directly proportional to the crystalline level of the carbon material [65]. The degree of graphitization of the carbon materials can be expressed by the I_D/I_G ratio calculated from the peak intensity of D and G bands. The peak ratio of DM 1, DM 2 and DM 3 are determined to be 0.86, 0.86 and 0.84, respectively. The smaller the I_D/I_G ratio, the higher the degree of graphitization with a low degree of amorphous, improves the electron transportability, reduce interfacial charge transfer resistance [66,67]. Activation of KOH in raw material can offer extra structural defects foremost to a superior degree of disorder [68].

The materials porosity is examined by N_2 adsorption at −196.15 °C and the data obtained for adsorption/desorption isotherms are shown in Fig. 2(c). The parameters of surface area and pore volume are summarized in Table 1. As exposed in Fig. 2(c) all the samples display type I and IV adsorption isotherms according to the IUPAC rule with obvious hysteresis loops at relatively higher pressure in P/P_0 range from 0.5 to 1, signifying the existence of abundant mesoporous embedded in the activated carbon samples [69–71]. The low and high activation temperature compared with the BET surface area and pore volume calculated by BJH method lie in the range of 10.5784 m^2/g and 0.054012 cm^3/g for DM 1 and DM 3 range to 795.4857 m^2/g and 0.395933 cm^3/g, respectively. Significantly, there is no collapse of the pore structure noticed with an increase in the activation temperature as shown in Fig. 2(d) ideal for ions movements enhance the superior performance of electrode.

The codoped AC of sample DM 1 with small number of activated sites, leading to a less porous and low surface area compared to DM 2 and DM 3 samples may be due to low activation temperature. The activation progress of DM 2 and DM 3 is sufficiently enhanced in development of high surface area and pore width corresponding with increasing temperature. The KOH/raw material(DM) weight ratio has significantly developed high surface area, pore width and the hysteresis loop adsorption curve at higher pressure profile. As it is believed that superior surface area of active material is essential for the permeability of electrolyte ions from side to side pores [72,73]. The calculated average pore diameter of DM 1, DM 2 and DM 3 are 10.4, 5.0 and 4.1 nm, respectively. The activation temperature and activating agent are significant factors for the formation of interstitial porosity and the results confirms the interparticle pores promoted the mesoporosity enhanced in sample DM 3 (600 °C) with pore size of 4 nm. These evidences clearly demonstrate the enhancement of KOH during the activation process. The amount of KOH and activation processes improves the surface area and pore volume of derived AC [74,75] afford for the transport of electrolyte ions which is beneficial in various applications [76–79].

HRSEM investigation was performed to obtain the detailed morphology in the low and high magnification SEM images as shown in Fig. S1 (a - i). From the perspective of the magnified SEM image, the morphology appears to be volcanic lava stone. Fig. S1 (a - c) shows image of DM 1 AC at activation temperature 400 °C, the stratum of AC is thick and densely compact with small pores at lower activation temperature, as activation temperature increases to 500 °C there are improved numerous porous network developed in the AC stratum as shown in Fig. S1 (d - f) exhibits DM 2 sample. Fig. S1 (g - i) shows the morphology of the sample DM 3 with higher activation temperature shows uniformly-distributed numerous porous network. At lower magnification, the SEM images shows porous nature of the carbon matrix in 1 and 2 μm, and higher magnification of SEM images at 500 nm display a numerous pores are created in the surface on the carbon matrix. Interestingly, DM 3 exhibits highly porous structure in the carbon matrix obtained. It is manifested that the activation temperature and activation agent KOH have successfully opened up porous structures in active materials. Additionally, the layers of carbon particle become smaller and plentiful round holes increases play a vital role in storage and transport ability. Moreover, the porous structure could be observed from the HRTEM image Fig. S2. The inset figure reveals disordered carbon matrix showing no interlayer distance, which is consistent with the corresponding Fast Fourier Transform (FFT) pattern obtained.

The addition of thiourea as the precursor for codoping results in the introduction of N, S atoms into the carbon structures of all the prepared samples. The contents of N and S heteroatoms in various carbon samples were determined by elemental mapping and summarized in Table 2. The sample DM 1 activated at 400 °C reported the highest weight percentages of codoped heteroatoms is 19.75 wt% (19% for N atom, 0.75% for S atom). The sample DM 2 activated at 500 °C reported the weight percentages of codoped heteroatoms is 10.22 wt% (5.75% for N atom, 4.47% for S atom) and sample DM 3 activated at 600 °C reported the moderate weight percentages of codoped heteroatoms is 6.23 wt% (5.03% for N atom, 1.2% for S atom) respectively. These weight percentages of codoped heteroatom in carbon matrix showed the level of doping at three activation temperature. From the Fig. S3 EDX graph of sample DM 3 with inset indicates the elements C, N, O and S have been successfully incorporated.

XPS was employment to authentic the surface functionalities of DM 3 and their corresponding spectra are shown in Fig. 3(a - d). Through XPS spectra, the surface functionalities of DM 3 were authenticated. Additionally, the comparison with DX mapping is show in Table 3. From XPS spectra the content of carbon is determined as 85.5 at.% is in accordance with those measured through EDX mapping shows 83.7 at.%. The level O doped by 10.07 at.% is in accordance with 10.03 at.%. The level N doped by 3.24 at.% is in accordance with 5.03 at.%. The level S doped by 1.23 at.% is in accordance with 1.2 at.% which reveals the presence of N, S elements codoped activated carbon. The fitted high-resolution carbon (C1s) spectrum shown in Fig. 3(a) can be deconvoluted into five peaks, 283.68, 284.21, 284.87, 285.65 and 287.58 ascribed to C-S-C, C-C/C = C, C-OH/C-H/C-S, C-N-C and C-O-C/O-C = O respectively. The presence of functionalities certainly creates wettability and pseudocapacitance, due to transfer kinetics of electron and admirable redox [80] . The fitted high-resolution oxygen (O1s) spectrum shown in Fig. 3(b) can be deconvoluted into four peaks, 530.99, 532.63, 534.73 and 536.95 eV ascribed to carbonyl groups C═O, C–O–C/C–OH, SO_x and H-O-H respectively [81]. The Fig. 3(d) shows

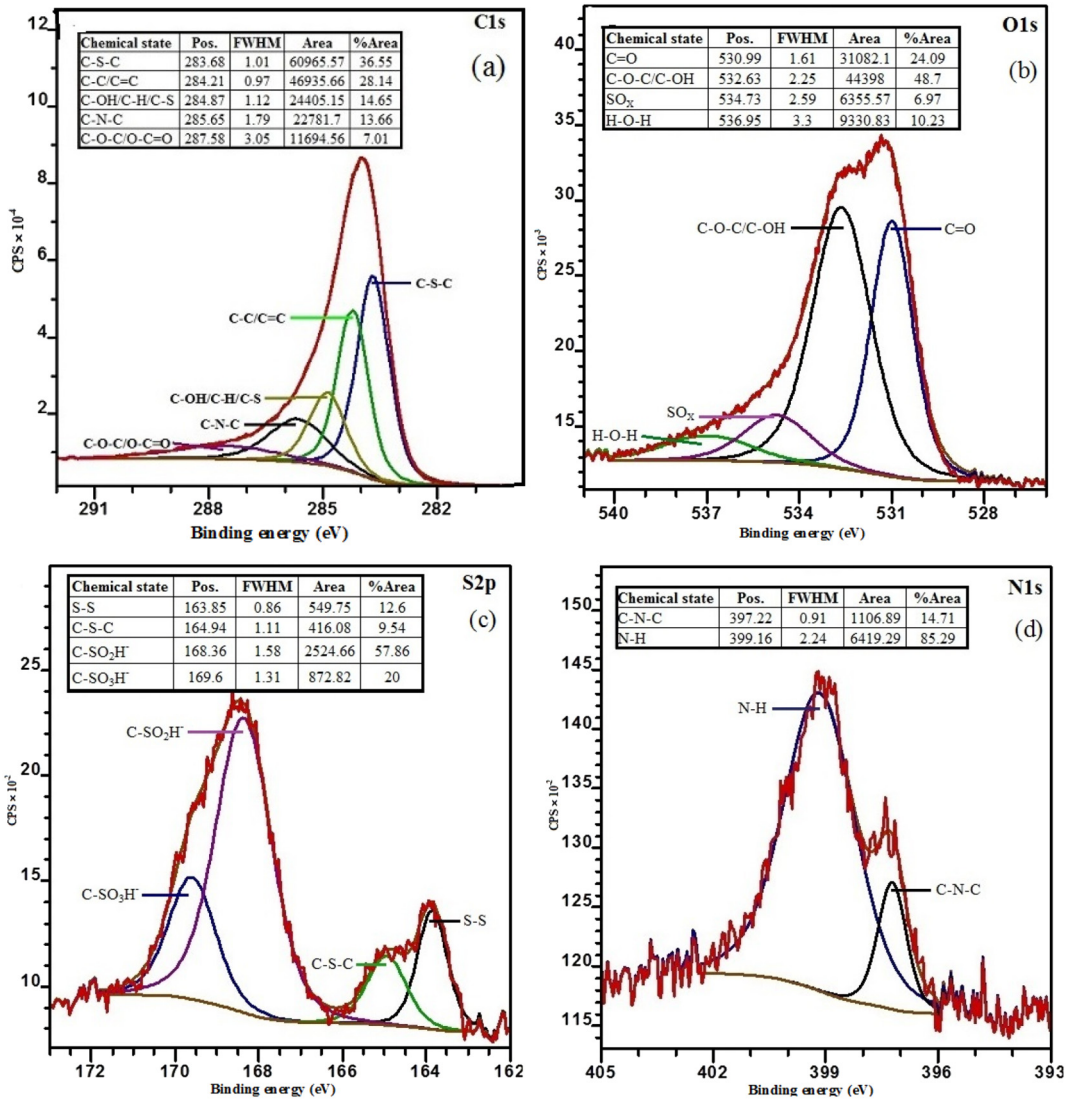

Fig. 3. XPS spectra of DM 3(a) deconvoluted C1s, (b) deconvoluted O1s, (d) deconvoluted N1s and (c) deconvoluted S2p.

high resolution N1s peaks are the chemical state of nitrogen's species on carbon matrix, the peaks at binding energies of 397.22 eV are assigned to pyridinic–N and pyrrolic–N (399.16 eV) [82]. The fitted high-resolution sulfur (S2p) spectrum shown in Fig. 3(c) can be alienated into two broad regions, the region from 162.0–166.3 eV is assigned to aromatic sulphide and one more region from 166.5–172 eV is assigned to oxidized sulfur, these regions are comprise of strong relations between S and C. The aromatic sulphide can be deconvoluted into two peaks, 163.85 and 164.94 eV, ascribed to $S2p_{3/2}$ attributed to S—S and $S2p_{1/2}$ attributed to C–S–C, arising from spine-orbit coupling respectively. The oxidized sulfur can be deconvoluted into two peaks, 168.36 and 169.60 eV attributing to($C\text{-}SO_xH^-$) sulphone bridges respectively [83] .

An electrochemical impedance spectroscopy (EIS) is a powerful tool to examine the charge transport and ion diffusion of DM working electrodes in 1 M H_2SO_4 aqueous solution. The Nyquist impedance spectra recorded with two regions between Z'' (imaginary axis) and Z' (real axis) obtained in a frequency range of 10 KHz to 1 mHz represented in Fig. 4. The Nyquist plots reveal DM 1 to DM 3 electrodes doesn't have same conductivity, besides their tempo of vary in wt% of functional group and their activation stipulation. From the Nyquist plots of DM 1, DM 2 and DM 3, particularly in the low frequency region shows almost vertical line, demonstrating idyllic behavior of a capacitor. The plots do not show any semicircle in this region, possibly

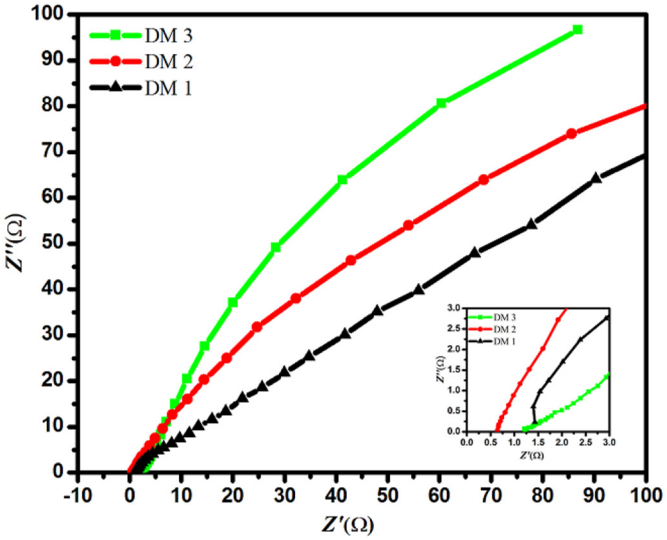

Fig. 4. Nyquist plots of DM 1, DM 2 and DM 3 electrodes in the frequency range of 10 KHz to 1mHz.

owing to its little Faradaic resistance [84]. From Nyquist plot, the slope of the line is connected to the development rate of the EDLC. Superior the slope value, the quicker the EDLC will be formed [85]. Thus, it can be accomplished that the N, S functionalities on the surface of AC labeled DM samples are greatly encouraging for the speedy development of EDLC, which agrees well with the CV measurements. In addition, the mid-frequency range slope portion of the curve is entitled to Warburg resistance, which is ascribed to ion diffusion and transport from electrolyte to the surface of electrode [86]. Fig. 4 inset, indicates a typical Warburg impedance showing DM 1, DM 2 and DM 3 are 1.6, 0.7 and 1.2 Ω, respectively.

To authenticate the working performance of derived N, S codoped AC materials from Datura metel seed pod was assembled in a three-electrode system. The testing includes cyclicvoltammetry and galvanostatic charge/discharge, the capacitive performances of the electrodes are explored in 1 M H_2SO_4 used as an electrolyte. The working electrodes of the labeled energetic materials tested in a potential window of 0.0–1.0 V at different scan rates ranging from 2, 5, 10, 20, 50, 75 and 100 mV/s, reveal the electrochemical nature of carbon material. The typical capacitive behaviors of the N, S codoped AC materials were revealed in Fig. 5(a - c). The working electrodes labeled as DM 1, DM 2 and DM 3 used in this study as energetic material displays CV curves of highly capacitive nature. The obtained CVs of the energetic material reveals completely distorted rectangular shape with redox active sites exhibited from carbonaceous materials associated from moderate N, S containing functional groups [87] and high surface area which reflects the arrangement of electric double layer capacitance and pseudocapacitance. With the rising activation temperature from 400 to 600 °C, the DM 3 electrode exhibit superior shape of CV curves among other, which exhibits almost rectangular trend. It is evident the areas with CV curves are clearly not alike. Such noticeable changes in the CV curves are almost certainly ascribed to their porous structures and cooped heteroatoms in the AC [88]. The current responses of all the working electrodes were studied, respectively. The specific capacitance is practically relative to the area of the CV shape [89] evidently, the working electrode DM 3 has a larger CV curve area than that of other working electrodes, consistent with the highest specific capacitance.

The CV curves of working electrode DM1 along with bare carbon felt are reported in Fig. 5 (a) shows the comparative CV traces of bare carbon felt scanned at 10 mV/s along with DM 1 working electrode scanned at different scan rate. The CV trends of bare carbon felt demonstrate far different from the working electrode DM 1, evidently the current response of bare carbon felt shows a negligible current response. CV traces of bare carbon felt scanned even at various scan rates in sort to find the current response of the same; seems to be poor performance and discharging time takes place even < 1 s, which relatively shows negligible effect in actual specific capacitance. Meanwhile, compared to the working electrodes DM 1 and DM 2, the enhanced DM 3 working electrode represents better-symmetric and rectangular CV curves evidenced at higher scan rates ascribed to N, S functionalities, a higher specific surface area and acute porous structure which supply lodging to electrolyte ions.

For deeper perceptive of capacitive behavior in relative to the CV curve, in particular at a scan rate of 5 mV/s in the same potential range is selected for the determination of comparative behavior of the working electrode of DM 1, DM 2 and DM 3 are shown in Fig. S4 (a) indicates a typical quasi rectangular shape ideal for EDLC. Similarly, GCD profile of working electrodes DM 2 and DM 3 are compared with their curve, in particular at a current density of 1 A/g in the same potential range indicates similar discharging curves are shown in Fig. S4 (b).

The GCD profile of working electrodes DM 2 and DM 3 exposes a triangular shape signifying distinctive galvanostatic charge/discharge curves, especially discharge curves express an arc-like contributing to the pseudofaradaic reactions [90]. As shown in Fig. 6 (a and b) contains GCD curves of derived N, S codoped AC for DM 2 and DM 3, at a variety

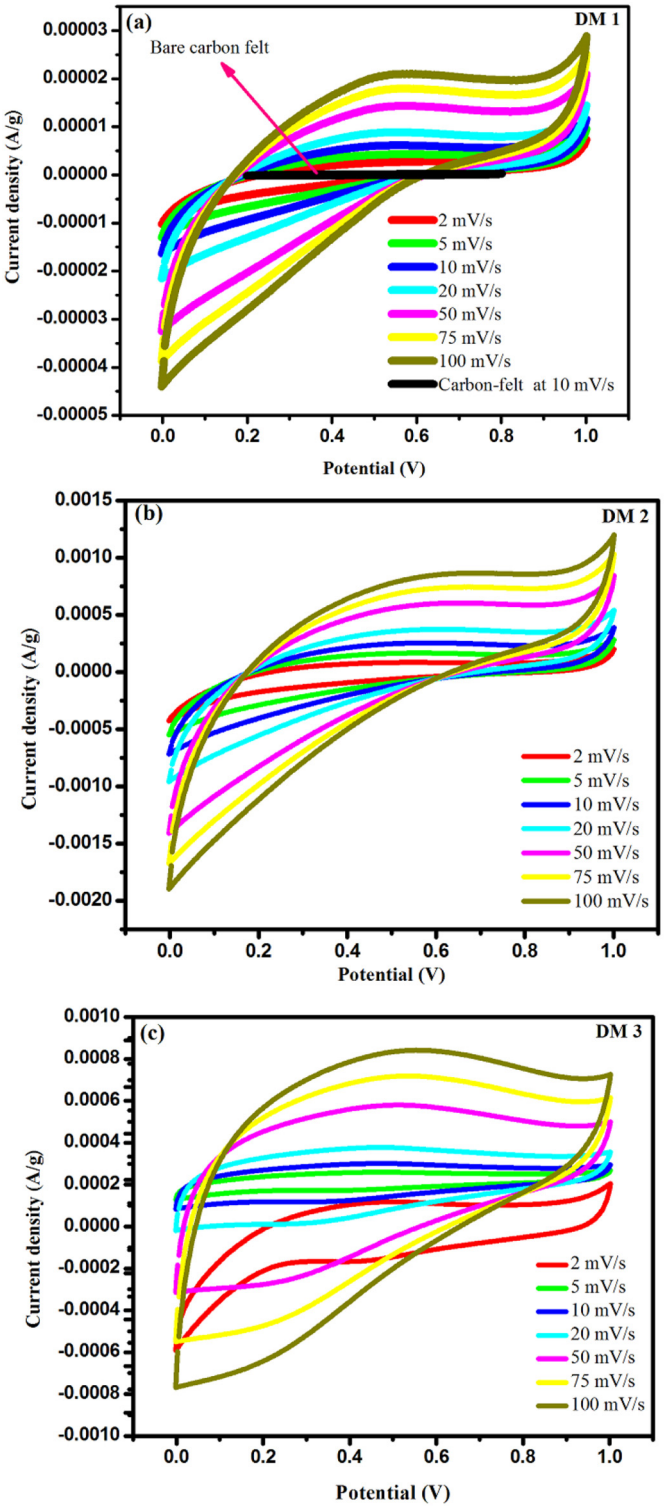

Fig. 5. Comparison of CV traces of N, S codoped AC (a) DM 1with bare carbon felt (b) DM 2 and (c) DM 3 at different scan rates (2, 5, 10, 20, 50, 75 and 100 mV/s).

of current densities range from 1, 2, 3, 4, 5 and 10 A/g, and the specific capacitances are calculated using Eq. (1) and the values are tabulated in Table 4 which illustrates the working electrode of energetic material DM 3 presenting high capacitive activities and well-balanced charge storage, contribute awesome capacitive behavior. The importance of moderate N, S functional groups in the AC modify the polarization of carbon matrixes because the carbon atoms adjoining to an N or S atom

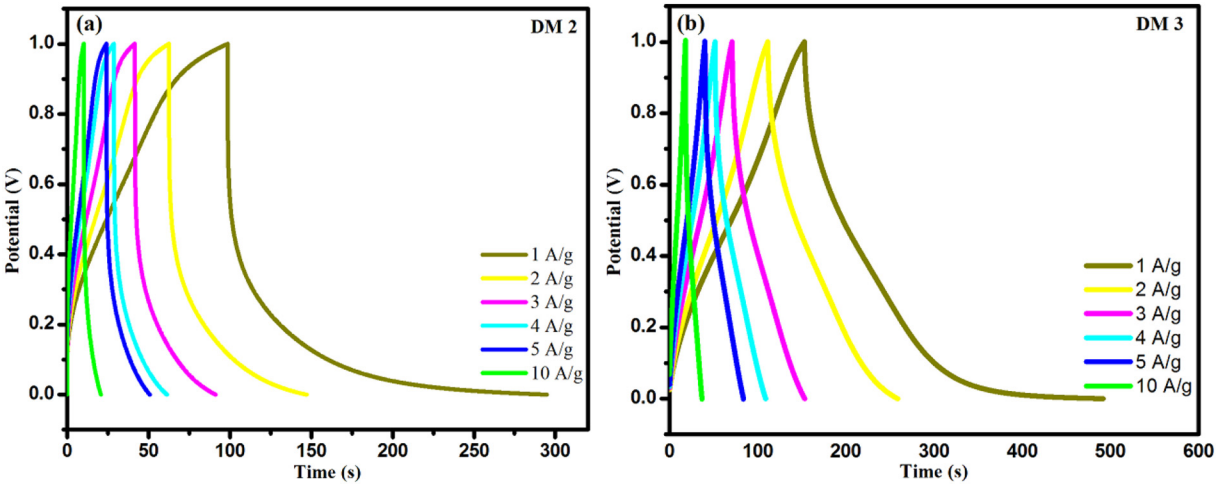

Fig. 6. Comparison of GCD traces of N, S codoped activated carbon (a) DM 2 and (b) DM 3 at different current densities (1, 2, 3, 4, 5 and 10 A/g).

acquire a notably positive charge solidity to recompense the sturdy electronic affinity of the N and S atoms, which improve the wettability of the carbon matrix. Therefore, improved electrode/electrolyte wettability can support ion diffusion at the interface between the electrolyte and electrode, thus improving the electrochemical performance [91].

The derived specific capacitances through galvanostatic charge/discharge for the working electrodes DM 2 and DM 3, display the excellent capacitance values of which DM 3 shows high specific capacitances of 340 F/g at 1A/g, respectively derived from Eq. (1), similarly the others are tabulated. These results suggest that the working electrode DM 3 possesses the highest capacitances compared to other working electrodes measured at 1 A/g current density. Further, the working electrode DM 3 reveals the superior capacitive performance obtained with established N, S codoping, high surface area and more suitable pore size distribution successfully increase the capacitance of the carbon material. Simultaneous in situ, at small current density of 1 A/g, the working electrode DM 3 exhibit the longest time to a comprehensive charge/discharge cycle. The time taken to discharge is higher than charging. This synergistic result is the novelty of the derived activated carbon from a Datura metel seed pod with the high capacitance of 340 F/g. An extraordinary association between the content of N and S incorporated into the carbon framework proves convincing specific capacitance value. The electrochemical properties of AC derived from Datura metel seed pod is compared with different biomass derived activated carbon electrode material and their electrochemical parameters are compared in Table 5.

To investigate the electrochemical stability, a long-term cycling test of DM 2 and DM 3 working electrodes is studied for 3000 charging-discharging cycles and represented in Fig. 7(a and b) with inset showing the first 5 cycles and last 5 cycles, exhibiting the capacitance retention of 85.53% and 95.24% at potential windows of 0.0–1.0 V, respectively. Fig. 7(c) demonstrates the rate performance measurements of DM 2 and DM 3, representing the specific capacitances with cycle number exhibiting performance of DM 2 and DM 3 at various current densities. Fig. 7 (d) shows the relationship between specific capacitance and current densities. These results further evidence the excellent cycle stability of DM 3 electrode.

Table 2
Elemental analysis of codoped AC samples.

Sample	DM 1		DM 2		DM 3	
Element	wt%	at.%	wt%	at.%	wt%	at.%
CK	73.68	77.41	77.83	83.32	82.32	83.7
NK	19	17.11	5.75	5.28	6.28	5.03
OK	6.57	5.18	11.95	9.61	9.61	10.03
SK	0.75	0.29	4.47	1.79	1.79	1.2

Table 3
Authentication of codoped atoms of DM 3 sample with EDX and XPS.

DM 3		
Elements	EDX	XPS
	At.%	At.%
CK	83.7	85.5
NK	5.03	3.24
OK	10.03	10.07
SK	1.2	1.23

Table 4
Specific capacitance of the samples DM 2 and DM 3 at different current densities.

Sample	Specific capacitance (F/g)					
	1 A/g	2 A/g	3 A/g	4 A/g	5 A/g	10 A/g
DM 2	196	170	150	136	130	110
DM 3	340	294	249	228	220	200

4. Conclusion

In summary, a novel N, S codoped AC mesoporous structure shows volcanic lava stone like morphology of the carbon matrix derived from

Table 1
Study of activation condition progress in the surface area and pore size.

Sample	Activation temperature (°C)	BET surface area (cm^3/g)	Pore volume (P/Po = 0.99) (m^2/g)	Pore width (Å)
DM 1	400	10.5784	0.054012	1424.425
DM 2	500	415.2237	0.249746	7.716
DM 3	600	795.4857	0.395933	5.651

Table 5
Comparison of electrochemical parameters of different biomass derived activated carbon electrodes.

Carbon source	Activating agent	Specific capacitance (F/g)	Current density	Electrolyte	Ref.
Argania spinosa (seed shell)	KOH/melamine	355	125 mA/g	1 M H_2SO_4	[92]
Bamboo	carbonization and KOH	293	0.5 A/g	3 M KOH	[93]
Neem dead leaves	No activation	400	0.5 A/g	1 M H_2SO_4	[94]
Sugarcane bagasse	$ZnCl_2$	300	250 mA/g	1 M H_2SO_4	[95]
Sunflower seed shell	KOH	311	250 mA/g	30 wt% KOH	[96]
Waste coffee beans	$ZnCl_2$	368	50 mA/g	1 M H_2SO_4	[97]
Datura metel seed pod	KOH	340	1 A/g	1 M H_2SO_4	present work

Datura metel seed pod was synthesized successfully by a simple hydrothermal process. The advantage of this simple preparation route, suggesting the high yield of activated mesoporous carbon could be obtained. The 30 wt% of KOH and addition of thiourea influenced a crucial role in the activation process, facilitate codoped N, S mesoporous architecture and ultrahigh surface area. The graphitic nature was confirmed by XRD and Raman spectra. DM 3 sample acquired a maximum surface area of 795.4857 m^2/g among all other samples was obtained by BET measurements. EDX and XPS evidenced the presence of N, S, C and O in the samples. The specific capacitance of 340 F/g at a current density of 1 A/g was attained for working electrode DM 3 via galvanostatic charge/discharge tests. Thus, Datura metel seed pod can be used as a prosepective choice for the synthesis of AC material for energy-storage based applications.

Authors' statement

I am submitting a manuscript which reports on N, S codoped activated mesoporous carbon derived from the **Datura metel seed pod** as active electrodes with the moderate intakes of Nitrogen and (N) sulfur (S) contents in the codoped AC process turned the materials to be a potential candidate for supercapacitor applications, this attempt explored the pioneer work in this species via hydrothermally. This codoped AC exhibits high specific capacitance of 340 F/g at a current density of 1 A/g. I assure you that the manuscript has not been published previously and it is not under consideration in any journal for publication elsewhere. Also the publication is approved by all authors and explicitly by the responsible authorities where the work was carried out. Submission also implies that, if accepted, it will not be

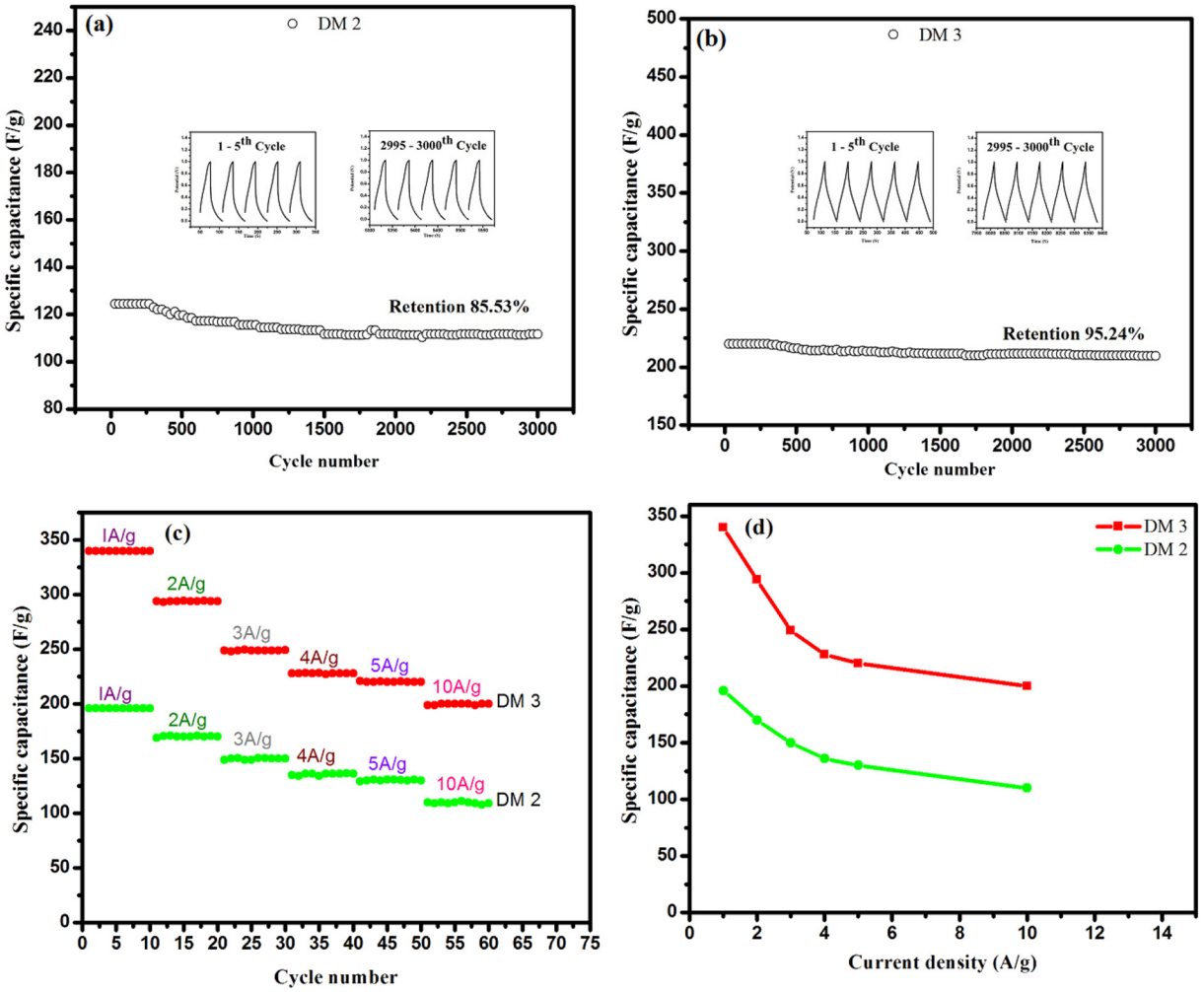

Fig. 7. Electrochemical performances of DM 2 and DM 3 using 1 M H_2SO_4 as electrolytes: (a) cycling stability of DM 2; (b) cycling stability of DM 3; (c) rate performance measurements and (d) the relationship between specific capacitance and current densities.

published elsewhere in the same form, in English or in any other language, without the written consent of the Publisher. It may kindly be considered in “Diamond and related materials” for publication.

Appendix A. Supplementary figures

- HRSEM image of samples from DM 1 to DM 3 at different magnifications
- EDX with elemental mapping of sample DM 3
- Comparative CV traces from DM 1 to DM 3 at a scan rate of 5 mV/s
- Comparative GCD profiles of electrodes DM 2 and DM 3 at a current density of 1 A/g

Supplementary figures to this article can be found online at https://doi.org/10.1016/j.diamond.2019.107687.

References

[1] Y. Lu, B. Li, S. Zheng, Y. Xu, H. Xue, H. Pang, Syntheses and energy storage applications of MxSy (M = Cu, Ag, Au) and their composites: rechargeable batteries and supercapacitors, Adv. Funct. Mater. 27 (44) (2017) 1703949.

[2] Y. Zhang, X. Rui, Y. Tang, Y. Liu, J. Wei, S. Chen, W.R. Leow, W. Li, Y. Liu, J. Deng, B. Ma, Q. Yan, X. Chen, Wet-chemical processing of phosphorus composite nanosheets for high-rate and high-capacity lithium-ion batteries, Adv. Energy Mater. 6 (10) (2016) 1502409.

[3] A.S. Aricò, P. Bruce, B. Scrosati, J.-M. Tarascon, W. van Schalkwijk, Nanostructured materials for advanced energy conversion and storage devices, Nat. Mater. 4 (2005) 366.

[4] S. Zheng, X. Li, B. Yan, Q. Hu, Y. Xu, X. Xiao, H. Xue, H. Pang, Transition-metal (Fe, Co, Ni) based metal-organic frameworks for electrochemical energy storage, Adv. Energy Mater. 7 (18) (2017) 1602733.

[5] D. Qi, Y. Liu, Z. Liu, L. Zhang, X. Chen, Design of architectures and materials in in-plane micro-supercapacitors: current status and future challenges, Adv. Mater. 29 (5) (2017) 1602802.

[6] J.R. Miller, P. Simon, Electrochemical capacitors for energy management, Science 321 (5889) (2008) 651–652.

[7] H. Wang, W. Yu, J. Shi, N. Mao, S. Chen, W. Liu, Biomass derived hierarchical porous carbons as high-performance anodes for sodium-ion batteries, Electrochim. Acta 188 (2016) 103–110.

[8] G. Ye, X. Zhu, S. Chen, D. Li, Y. Yin, Y. Lu, S. Komarneni, D. Yang, Nanoscale engineering of nitrogen-doped carbon nanofiber aerogels for enhanced lithium ion storage, J. Mater. Chem. A 5 (18) (2017) 8247–8254.

[9] Nanogenerators: an emerging technology towards nanoenergy, APL Materials 5 (7) (2017) 074103.

[10] Y. Wang, Y. Song, Y. Xia, Electrochemical capacitors: mechanism, materials, systems, characterization and applications, Chem. Soc. Rev. 45 (21) (2016) 5925–5950.

[11] M. Armand, J.M. Tarascon, Building better batteries, Nature 451 (2008) 652.

[12] P. Simon, Y. Gogotsi, Materials for electrochemical capacitors, Nat. Mater. 7 (2008) 845.

[13] J. Hou, C. Cao, F. Idrees, X. Ma, Hierarchical porous nitrogen-doped carbon nanosheets derived from silk for ultrahigh-capacity battery anodes and supercapacitors, ACS Nano 9 (3) (2015) 2556–2564.

[14] L. Kou, T. Huang, B. Zheng, Y. Han, X. Zhao, K. Gopalsamy, H. Sun, C. Gao, Coaxial wet-spun yarn supercapacitors for high-energy density and safe wearable electronics, Nat. Commun. 5 (2014) 3754.

[15] H.D. Yoo, E. Markevich, G. Salitra, D. Sharon, D. Aurbach, On the challenge of developing advanced technologies for electrochemical energy storage and conversion, Mater. Today 17 (3) (2014) 110–121.

[16] K.P. Singh, D. Bhattacharjya, F. Razmjooei, J.-S. Yu, Effect of pristine graphene incorporation on charge storage mechanism of three-dimensional graphene oxide: superior energy and power density retention, Sci. Rep. 6 (2016) 31555.

[17] N.K. Chaudhari, S. Chaudhari, J.-S. Yu, Cube-like α-Fe2O3 supported on ordered multimodal porous carbon as high performance electrode material for supercapacitors, ChemSusChem 7 (11) (2014) 3102–3111.

[18] X.-Y. Zhao, J.-P. Cao, K. Morishita, J.-i. Ozaki, T. Takarada, Electric double-layer capacitors from activated carbon derived from black liquor, Energy Fuel 24 (3) (2010) 1889–1893.

[19] J. Zhang, J. Jiang, H. Li, X.S. Zhao, A high-performance asymmetric supercapacitor fabricated with graphene-based electrodes, Energy Environ. Sci. 4 (10) (2011) 4009–4015.

[20] K. Qin, J. Kang, J. Li, C. Shi, Y. Li, Z. Qiao, N. Zhao, Free-standing porous carbon nanofiber/ultrathin graphite hybrid for flexible solid-state supercapacitors, ACS Nano 9 (1) (2015) 481–487.

[21] K. Qin, J. Kang, J. Li, E. Liu, C. Shi, Z. Zhang, X. Zhang, N. Zhao, Continuously hierarchical nanoporous graphene film for flexible solid-state supercapacitors with excellent performance, Nano Energy 24 (2016) 158–164.

[22] K. Qin, E. Liu, J. Li, J. Kang, C. Shi, C. He, F. He, N. Zhao, Supercapacitors: free-standing 3D nanoporous duct-like and hierarchical nanoporous graphene films for micron-level flexible solid-state asymmetric supercapacitors (Adv. Energy Mater. 18/2016), Adv. Energy Mater. 6 (18) (2016).

[23] Z. Wen, X. Wang, S. Mao, Z. Bo, H. Kim, S. Cui, G. Lu, X. Feng, J. Chen, Crumpled nitrogen-doped graphene nanosheets with ultrahigh pore volume for high-performance supercapacitor, Adv. Mater. 24 (41) (2012) 5610–5616.

[24] B. You, L. Wang, N. Li, C. Zheng, Improving the energy storage performance of graphene through insertion of pristine CNTs and ordered mesoporous carbon coating, ChemElectroChem 1 (4) (2014) 772–778.

[25] T.B. Schon, P.M. DiCarmine, D.S. Seferos, Polyfullerene electrodes for high power supercapacitors, Adv. Energy Mater. 4 (7) (2014) 1301509.

[26] J. Ge, H.-B. Yao, W. Hu, X.-F. Yu, Y.-X. Yan, L.-B. Mao, H.-H. Li, S.-S. Li, S.-H. Yu, Facile dip coating processed graphene/MnO2 nanostructured sponges as high performance supercapacitor electrodes, Nano Energy 2 (4) (2013) 505–513.

[27] Y. Shao, M.F. El-Kady, C.-W. Lin, G. Zhu, K.L. Marsh, J.Y. Hwang, Q. Zhang, Y. Li, H. Wang, R.B. Kaner, 3D freeze-casting of cellular graphene films for ultrahigh-power-density supercapacitors, Adv. Mater. 28 (31) (2016) 6719–6726.

[28] C. Guan, Z. Zeng, X. Li, X. Cao, Y. Fan, X. Xia, G. Pan, H. Zhang, H.J. Fan, Atomic-layer-deposition-assisted formation of carbon nanoflakes on metal oxides and energy storage application, Small 10 (2) (2014) 300–307.

[29] C. Zequine, C.K. Ranaweera, Z. Wang, S. Singh, P. Tripathi, O.N. Srivastava, B.K. Gupta, K. Ramasamy, P.K. Kahol, P.R. Dvornic, R.K. Gupta, High performance and flexible supercapacitors based on carbonized bamboo fibers for wide temperature applications, Sci. Rep. 6 (2016) 31704.

[30] L. Zhao, L.-Z. Fan, M.-Q. Zhou, H. Guan, S. Qiao, M. Antonietti, M.-M. Titirici, Nitrogen-containing hydrothermal carbons with superior performance in supercapacitors, Adv. Mater. 22 (45) (2010) 5202–5206.

[31] L.-L. Zhang, H.-H. Li, Y.-H. Shi, C.-Y. Fan, X.-L. Wu, H.-F. Wang, H.-Z. Sun, J.-P. Zhang, A novel layered sedimentary rocks structure of the oxygen-enriched carbon for ultrahigh-rate-performance supercapacitors, ACS Appl. Mater. Interfaces 8 (6) (2016) 4233–4241.

[32] D.-D. Zhou, W.-Y. Li, X.-L. Dong, Y.-G. Wang, C.-X. Wang, Y.-Y. Xia, A nitrogen-doped ordered mesoporous carbon nanofiber array for supercapacitors, J. Mater. Chem. A 1 (29) (2013) 8488–8496.

[33] L.-F. Chen, X.-D. Zhang, H.-W. Liang, M. Kong, Q.-F. Guan, P. Chen, Z.-Y. Wu, S.-H. Yu, Synthesis of nitrogen-doped porous carbon nanofibers as an efficient electrode material for supercapacitors, ACS Nano 6 (8) (2012) 7092–7102.

[34] Y. Jin, K. Tian, L. Wei, X. Zhang, X. Guo, Hierarchical porous microspheres of activated carbon with a high surface area from spores for electrochemical double-layer capacitors, J. Mater. Chem. A 4 (41) (2016) 15968–15979.

[35] X. Yang, J. Yu, W. Zhang, G. Zhang, Mesopore-dominant wormhole-like carbon with high supercapacitive performance in organic electrolyte, RSC Adv. 7 (25) (2017) 15096–15101.

[36] E.A. Ekimov, V.A. Sidorov, E.D. Bauer, N.N. Mel'nik, N.J. Curro, J.D. Thompson, S.M. Stishov, Superconductivity in diamond, Nature 428 (2004) 542.

[37] X. Sun, Y. Zhang, P. Song, J. Pan, L. Zhuang, W. Xu, W. Xing, Fluorine-doped carbon blacks: highly efficient metal-free electrocatalysts for oxygen reduction reaction, ACS Catal. 3 (8) (2013) 1726–1729.

[38] J.L. Fajardo-Díaz, F. López-Urías, E. Muñoz-Sandoval, Wrinkled nitrogen-doped carbon belts, Sci. Rep. 8 (1) (2018) 3546.

[39] W. Lei, Y.-P. Deng, G. Li, Z.P. Cano, X. Wang, D. Luo, Y. Liu, D. Wang, Z. Chen, Two-dimensional phosphorus-doped carbon nanosheets with tunable porosity for oxygen reactions in zinc-air batteries, ACS Catal. 8 (3) (2018) 2464–2472.

[40] H.J. Yoon, S.K. Hong, M.E. Lee, J. Hwang, H.-J. Jin, Y.S. Yun, Sulfur-doped carbon nanotemplates for sodium metal anodes, ACS Applied Energy Materials 1 (5) (2018) 1846–1852.

[41] J. Yang, M. Xu, J. Wang, S. Jin, B. Tan, A facile approach to prepare multiple heteroatom-doped carbon materials from imine-linked porous organic polymers, Sci. Rep. 8 (1) (2018) 4200.

[42] W. Yang, W. Yang, A. Song, L. Gao, L. Su, G. Shao, Supercapacitance of nitrogen-sulfur-oxygen co-doped 3D hierarchical porous carbon in aqueous and organic electrolyte, J. Power Sources 359 (2017) 556–567.

[43] X. Gong, S. Liu, C. Ouyang, P. Strasser, R. Yang, Nitrogen- and phosphorus-doped biocarbon with enhanced electrocatalytic activity for oxygen reduction, ACS Catal. 5 (2) (2015) 920–927.

[44] J. Wu, X. Zheng, C. Jin, J. Tian, R. Yang, Ternary doping of phosphorus, nitrogen, and sulfur into porous carbon for enhancing electrocatalytic oxygen reduction, Carbon 92 (2015) 327–338.

[45] D. Zhang, M. Han, Y. Li, L. Lei, Y. Shang, K. Wang, Y. Wang, Z. Zhang, X. Zhang, H. Feng, Phosphorus and sulfur dual doped hierarchic porous carbons with superior supercapacitance performance, Electrochim. Acta 222 (2016) 141–148.

[46] F. Su, X.S. Zhao, Y. Wang, J. Zeng, Z. Zhou, J.Y. Lee, Synthesis of graphitic ordered macroporous carbon with a three-dimensional interconnected pore structure for electrochemical applications, J. Phys. Chem. B 109 (43) (2005) 20200–20206.

[47] M. El-Merraoui, M. Aoshima, K. Kaneko, Micropore size distribution of activated carbon fiber using the density functional theory and other methods, Langmuir 16 (9) (2000) 4300–4304.

[48] Z. Said, A. Allagui, M.A. Abdelkareem, A.S. Elwakil, H. Alawadhi, R. Zannerni, K. Elsaid, Modulating the energy storage of supercapacitors by mixing close-to-ideal and far-from-ideal capacitive carbon nanofibers, Electrochim. Acta 301 (2019) 465–471.

[49] J. Fang, X. Miao, X. Zhang, Y. Liu, S. Chen, Y. Chen, W. Wang, Y. Zhang, Enhancing the capacity of activated carbon electrodes by a redox mediator pair for the fabrication of flexible asymmetric solid-state supercapacitors, J. Power Sources 418 (2019) 24–32.

[50] A. Borenstein, O. Hanna, R. Attias, S. Luski, T. Brousse, D. Aurbach, Carbon-based composite materials for supercapacitor electrodes: a review, J. Mater. Chem. A 5 (25) (2017) 12653–12672.

[51] A.G. Pandolfo, A.F. Hollenkamp, Carbon properties and their role in supercapacitors, J. Power Sources 157 (1) (2006) 11–27.
[52] S.J. Beynon, S. Chaturvedi, Datura intoxication in an adolescent male: a challenge in the internet era, J. Paediatr. Child Health 54 (1) (2018) 84–87.
[53] Y. Teng, E. Liu, R. Ding, K. Liu, R. Liu, L. Wang, Z. Yang, H. Jiang, Bean dregs-based activated carbon/copper ion supercapacitors, Electrochim. Acta 194 (2016) 394–404.
[54] M. Sevilla, A.B. Fuertes, Fabrication of porous carbon monoliths with a graphitic framework, Carbon 56 (2013) 155–166.
[55] F. Razmjooei, K. Singh, T.H. Kang, N. Chaudhari, J. Yuan, J.-S. Yu, Urine to highly porous heteroatom-doped carbons for supercapacitor: a value added journey for human waste, Sci. Rep. 7 (1) (2017) 10910.
[56] S.K. Singh, H. Prakash, M.J. Akhtar, K.K. Kar, Lightweight and high-performance microwave absorbing heteroatom-doped carbon derived from chicken feather fibers, ACS Sustain. Chem. Eng. 6 (4) (2018) 5381–5393.
[57] Y. Gong, D. Li, C. Luo, Q. Fu, C. Pan, Highly porous graphitic biomass carbon as advanced electrode materials for supercapacitors, Green Chem. 19 (17) (2017) 4132–4140.
[58] X.-X. Peng, Y.-Q. Lu, L.-L. Zhou, T. Sheng, S.-Y. Shen, H.-G. Liao, L. Huang, J.-T. Li, S.-G. Sun, Graphitized porous carbon materials with high sulfur loading for lithium-sulfur batteries, Nano Energy 32 (2017) 503–510.
[59] Y. Ma, J. Zhao, L. Zhang, Y. Zhao, Q. Fan, X.a. Li, Z. Hu, W. Huang, The production of carbon microtubes by the carbonization of catkins and their use in the oxygen reduction reaction, Carbon 49 (15) (2011) 5292–5297.
[60] W. Qian, F. Sun, Y. Xu, L. Qiu, C. Liu, S. Wang, F. Yan, Human hair-derived carbon flakes for electrochemical supercapacitors, Energy Environ. Sci. 7 (1) (2014) 379–386.
[61] J. Yu, M. Guo, F. Muhammad, A. Wang, F. Zhang, Q. Li, G. Zhu, One-pot synthesis of highly ordered nitrogen-containing mesoporous carbon with resorcinol–urea–formaldehyde resin for CO2 capture, Carbon 69 (2014) 502–514.
[62] A.J. Romero-Anaya, M. Ouzzine, M.A. Lillo-Ródenas, A. Linares-Solano, Spherical carbons: synthesis, characterization and activation processes, Carbon 68 (2014) 296–307.
[63] A.C. Ferrari, J. Robertson, Resonant Raman spectroscopy of disordered, amorphous, and diamondlike carbon, Phys. Rev. B 64 (7) (2001) 075414.
[64] S. Shrestha, N. Morse, W.E. Mustain, Effect of surface chemistry on the double layer capacitance of polypyrrole-derived ordered mesoporous carbon, RSC Adv. 4 (87) (2014) 47039–47046.
[65] V. Etacheri, C. Wang, M.J. O'Connell, C.K. Chan, V.G. Pol, Porous carbon sphere anodes for enhanced lithium-ion storage, J. Mater. Chem. A 3 (18) (2015) 9861–9868.
[66] L. Sun, C. Tian, Y. Fu, Y. Yang, J. Yin, L. Wang, H. Fu, Nitrogen-doped porous graphitic carbon as an excellent electrode material for advanced supercapacitors, Chem. Eur. J. 20 (2) (2014) 564–574.
[67] P. Hao, Z. Zhao, J. Tian, H. Li, Y. Sang, G. Yu, H. Cai, H. Liu, C.P. Wong, A. Umar, Hierarchical porous carbon aerogel derived from bagasse for high performance supercapacitor electrode, Nanoscale 6 (20) (2014) 12120–12129.
[68] Y. Huang, L. Peng, Y. Liu, G. Zhao, J.Y. Chen, G. Yu, Biobased nano porous active carbon fibers for high-performance supercapacitors, ACS Appl. Mater. Interfaces 8 (24) (2016) 15205–15215.
[69] M. Zhou, F. Pu, Z. Wang, S. Guan, Nitrogen-doped porous carbons through KOH activation with superior performance in supercapacitors, Carbon 68 (2014) 185–194.
[70] T. Smith, R.S. Rana, P. Missiaen, K.D. Rose, A. Sahni, H. Singh, L. Singh, High bat (*Chiroptera*) diversity in the early Eocene of India, Naturwissenschaften 94 (12) (2007) 1003–1009.
[71] J.C. Groen, L.A.A. Peffer, J. Pérez-Ramírez, Pore size determination in modified micro- and mesoporous materials. Pitfalls and limitations in gas adsorption data analysis, Microporous Mesoporous Mater. 60 (1) (2003) 1–17.
[72] M.Y. Song, H.Y. Park, D.-S. Yang, D. Bhattacharjya, J.-S. Yu, Seaweed-derived heteroatom-doped highly porous carbon as an electrocatalyst for the oxygen reduction reaction, ChemSusChem 7 (6) (2014) 1755–1763.
[73] K.P. Singh, M.Y. Song, J.-S. Yu, Iodine-treated heteroatom-doped carbon: conductivity driven electrocatalytic activity, J. Mater. Chem. A 2 (42) (2014) 18115–18124.
[74] P. Pachfule, D. Shinde, M. Majumder, Q. Xu, Fabrication of carbon nanorods and graphene nanoribbons from a metal–organic framework, Nat. Chem. 8 (2016) 718.
[75] Y. Zhu, S. Murali, M.D. Stoller, K.J. Ganesh, W. Cai, P.J. Ferreira, A. Pirkle, R.M. Wallace, K.A. Cychosz, M. Thommes, D. Su, E.A. Stach, R.S. Ruoff, Carbon-based supercapacitors produced by activation of graphene, Science 332 (6037) (2011) 1537–1541.
[76] H. Wei, H. Chen, N. Fu, J. Chen, G. Lan, W. Qian, Y. Liu, H. Lin, S. Han, Excellent electrochemical properties and large CO2 capture of nitrogen-doped activated porous carbon synthesised from waste longan shells, Electrochim. Acta 231 (2017) 403–411.
[77] C. Ma, X. Chen, D. Long, J. Wang, W. Qiao, L. Ling, High-surface-area and high-nitrogen-content carbon microspheres prepared by a pre-oxidation and mild KOH activation for superior supercapacitor, Carbon 118 (2017) 699–708.
[78] M. Sevilla, R. Mokaya, Energy storage applications of activated carbons: supercapacitors and hydrogen storage, Energy Environ. Sci. 7 (4) (2014) 1250–1280.
[79] D. Kang, Q. Liu, J. Gu, Y. Su, W. Zhang, D. Zhang, "Egg-box"-assisted fabrication of porous carbon with small mesopores for high-rate electric double layer capacitors, ACS Nano 9 (11) (2015) 11225–11233.
[80] Z. Song, D. Zhu, L. Li, T. Chen, H. Duan, Z. Wang, Y. Lv, W. Xiong, M. Liu, L. Gan, Ultrahigh energy density of a N, O codoped carbon nanosphere based all-solid-state symmetric supercapacitor, J. Mater. Chem. A 7 (3) (2019) 1177–1186.
[81] E. Hao, W. Liu, S. Liu, Y. Zhang, H. Wang, S. Chen, F. Cheng, S. Zhao, H. Yang, Rich sulfur doped porous carbon materials derived from ginkgo leaves for multiple electrochemical energy storage devices, J. Mater. Chem. A 5 (5) (2017) 2204–2214.
[82] J. Qu, C. Geng, S. Lv, G. Shao, S. Ma, M. Wu, Nitrogen, oxygen and phosphorus decorated porous carbons derived from shrimp shells for supercapacitors, Electrochim. Acta 176 (2015) 982–988.
[83] R. Atchudan, T.N.J.I. Edison, S. Perumal, A.S. Parveen, Y.R. Lee, Electrocatalytic and energy storage performance of bio-derived sulphur-nitrogen-doped carbon, J. Electroanal. Chem. 833 (2019) 357–369.
[84] Q. Wu, Y. Xu, Z. Yao, A. Liu, G. Shi, Supercapacitors based on flexible graphene/polyaniline nanofiber composite films, ACS Nano 4 (4) (2010) 1963–1970.
[85] W.-C. Chen, T.-C. Wen, H. Teng, Polyaniline-deposited porous carbon electrode for supercapacitor, Electrochim. Acta 48 (6) (2003) 641–649.
[86] H. Peng, G. Ma, K. Sun, J. Mu, Z. Zhang, Z. Lei, Formation of carbon nanosheets via simultaneous activation and catalytic carbonization of macroporous anion-exchange resin for supercapacitors application, ACS Appl. Mater. Interfaces 6 (23) (2014) 20795–20803.
[87] L. Zhao, L.-Z. Fan, M.-Q. Zhou, H. Guan, S. Qiao, M. Antonietti, M.-M. Titirici, Nitrogen-Containing Hydrothermal Carbons with Superior Performance in Supercapacitors, (2010).
[88] D. Hulicova-Jurcakova, M. Seredych, G.Q. Lu, N.K.A.C. Kodiweera, P.E. Stallworth, S. Greenbaum, T.J. Bandosz, Effect of surface phosphorus functionalities of activated carbons containing oxygen and nitrogen on electrochemical capacitance, Carbon 47 (6) (2009) 1576–1584.
[89] G. Boopathi, G.G. Karthikeyan, S.M. Jaimohan, A. Pandurangan, A.L.F. de Barros, Dopant effects of Gd3+ on the electrochemical pseudocapacitive characteristics of electroactive mesoporous NiO electrodes for supercapacitors, J. Phys. Chem. C 122 (17) (2018) 9257–9274.
[90] D. Hulicova-Jurcakova, M. Seredych, G.Q. Lu, T.J. Bandosz, Combined effect of nitrogen- and oxygen-containing functional groups of microporous activated carbon on its electrochemical performance in supercapacitors, Adv. Funct. Mater. 19 (3) (2009) 438–447.
[91] M. Kotal, H. Kim, S. Roy, I.-K. Oh, Sulfur and nitrogen co-doped holey graphene aerogel for structurally resilient solid-state supercapacitors under high compressions, J. Mater. Chem. A 5 (33) (2017) 17253–17266.
[92] A. Elmouwahidi, Z. Zapata-Benabithe, F. Carrasco-Marín, C. Moreno-Castilla, Activated carbons from KOH-activation of argan (Argania spinosa) seed shells as supercapacitor electrodes, Bioresour. Technol. 111 (2012) 185–190.
[93] G. Zhang, Y. Chen, Y. Chen, H. Guo, Activated biomass carbon made from bamboo as electrode material for supercapacitors, Mater. Res. Bull. 102 (2018) 391–398.
[94] M. Biswal, A. Banerjee, M. Deo, S. Ogale, From dead leaves to high energy density supercapacitors, Energy Environ. Sci. 6 (4) (2013) 1249–1259.
[95] T.E. Rufford, D. Hulicova-Jurcakova, K. Khosla, Z. Zhu, G.Q. Lu, Microstructure and electrochemical double-layer capacitance of carbon electrodes prepared by zinc chloride activation of sugar cane bagasse, J. Power Sources 195 (3) (2010) 912–918.
[96] X. Li, W. Xing, S. Zhuo, J. Zhou, F. Li, S.-Z. Qiao, G.-Q. Lu, Preparation of capacitor's electrode from sunflower seed shell, Bioresour. Technol. 102 (2) (2011) 1118–1123.
[97] T.E. Rufford, D. Hulicova-Jurcakova, Z. Zhu, G.Q. Lu, Nanoporous carbon electrode from waste coffee beans for high performance supercapacitors, Electrochem. Commun. 10 (10) (2008) 1594–1597.